Tailoring Chloride Solid Electrolytes for Reversible Redox

Phillip Ridley[a], George Duon[1a], Sarah L. Ko[b], Jin An Sam Oh[a], Grayson Deysher[c], Kent J. Griffith[b,c], Ying Shirley Meng[a,d*]*

AUTHOR ADDRESS

[a]Department of Nano Engineering, University of California San Diego, La Jolla, CA 92093, USA

[b]Department of Chemistry and Biochemistry, University of California, San Diego, CA 92093, USA

[c]Program of Materials Science and Engineering, University of California San Diego, La Jolla, CA 92093, USA

[d]Pritzker School of Molecular Engineering, The University of Chicago, Chicago, IL 60637, USA

AUTHOR INFORMATION

Corresponding Author

*Kent Griffith. Email: k3griffith@ucsd.edu

*Ying Shirley Meng. Email: shirleymeng@uchicago.edu

FIGURES

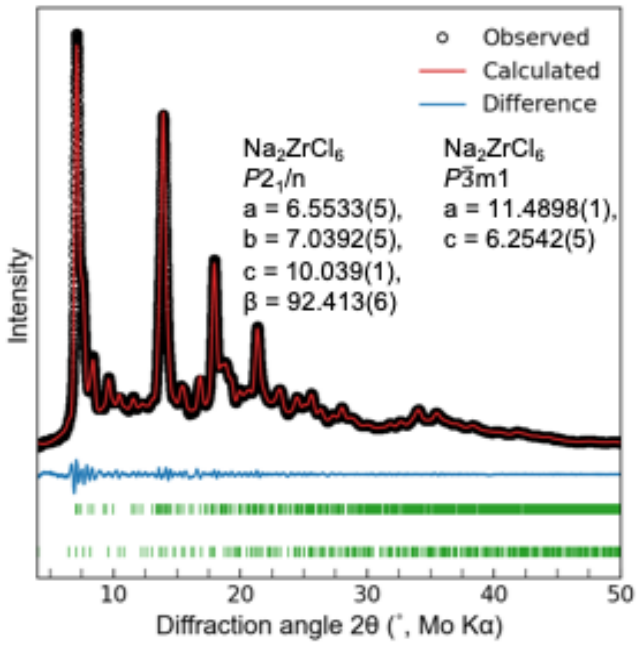

Supplementary Figure S1. Le Bail intensity fitting results for the Na_2ZrCl_6 end-member, using $P2_1/n$ and $P\bar{3}m1$ space group models.

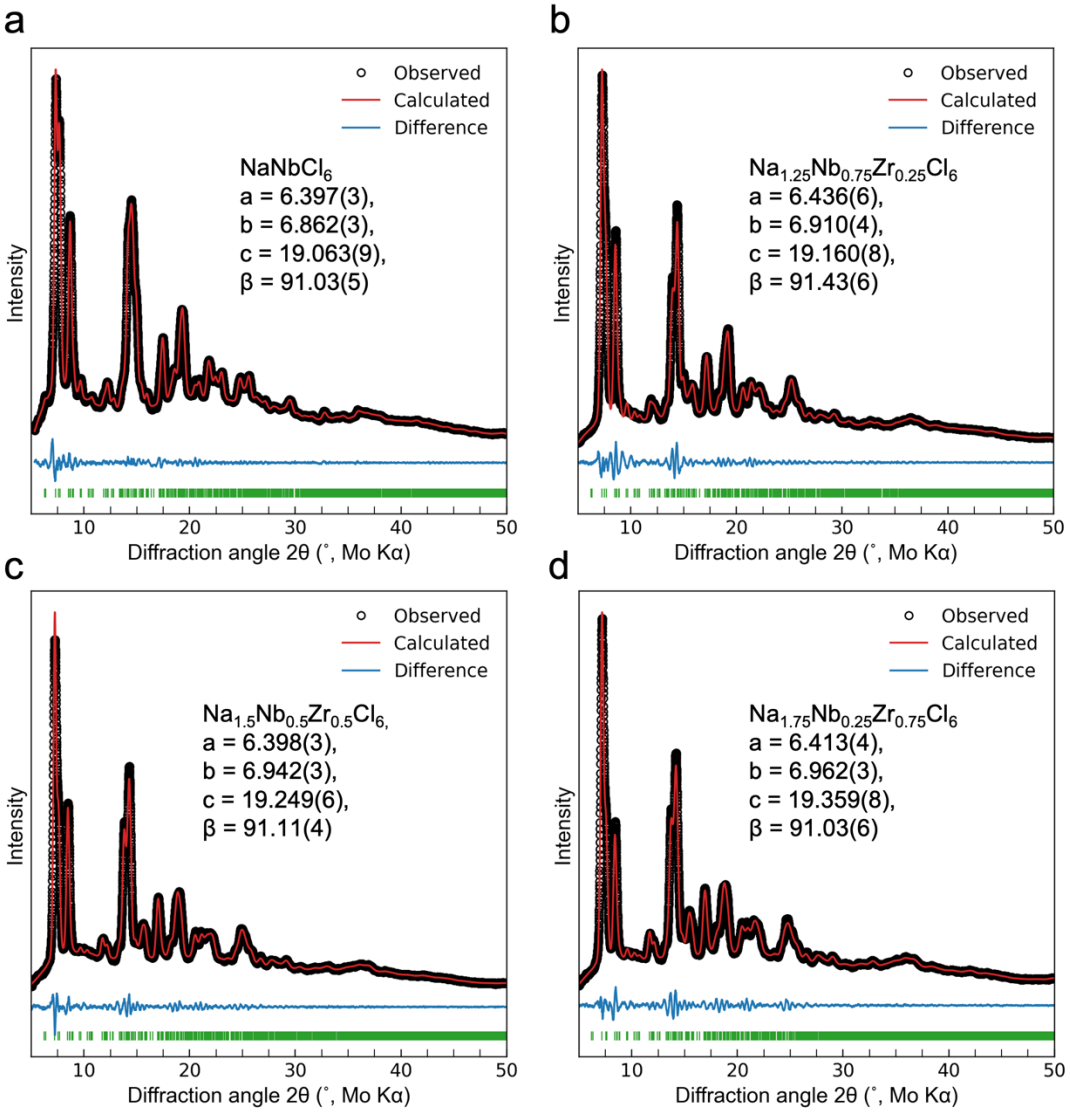

Supplementary Figure S2. Le Bail intensity fitting results for Nb-substituted $Na_{2-x}Nb_xZr_{1-x}Cl_6$ (x = 1, 0.75, 0.5, 0.25) solid-solutions.

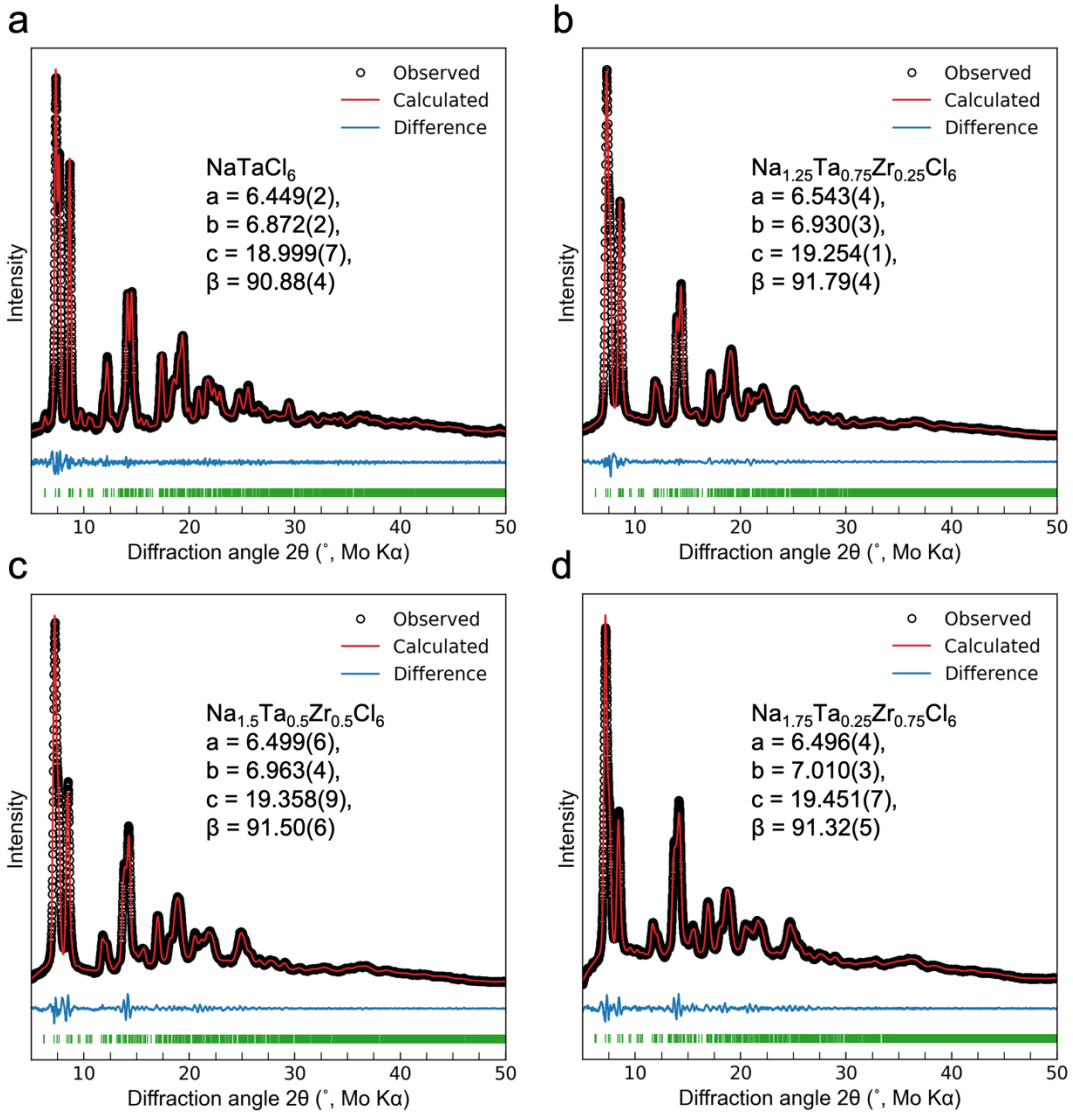

Supplementary Figure S3. Le Bail intensity fitting results for Ta-substituted $Na_{2-x}Ta_xZr_{1-x}Cl_6$ (x = 1, 0.75, 0.5, 0.25) solid-solutions.

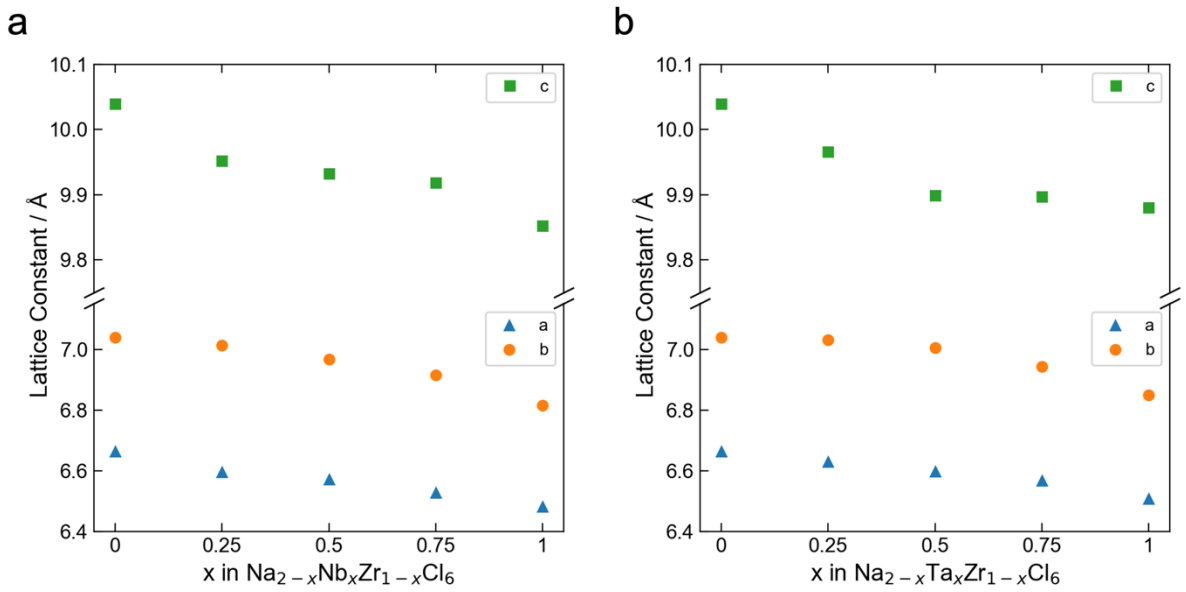

Supplementary Figure S4. Lattice constants extracted from Le Bail fits for a) $Na_{2-x}Nb_xZr_{1-x}Cl_6$ (x = 1, 0.75, 0.5, 0.25) and b) $Na_{2-x}Ta_xZr_{1-x}Cl_6$ (x = 1, 0.75, 0.5, 0.25) solid-solutions. Estimated standard deviations were too small to be graphically represented and are omitted.

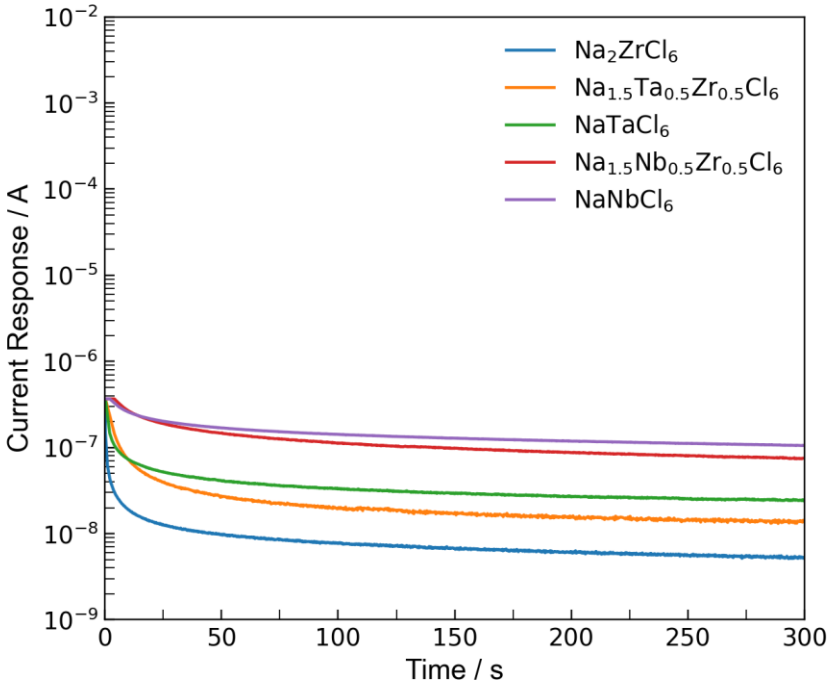

Supplementary Figure S5. Direct current polarization results for Nb-substituted and Ta-substituted solid-solutions collected using an applied bias of 50 mV.

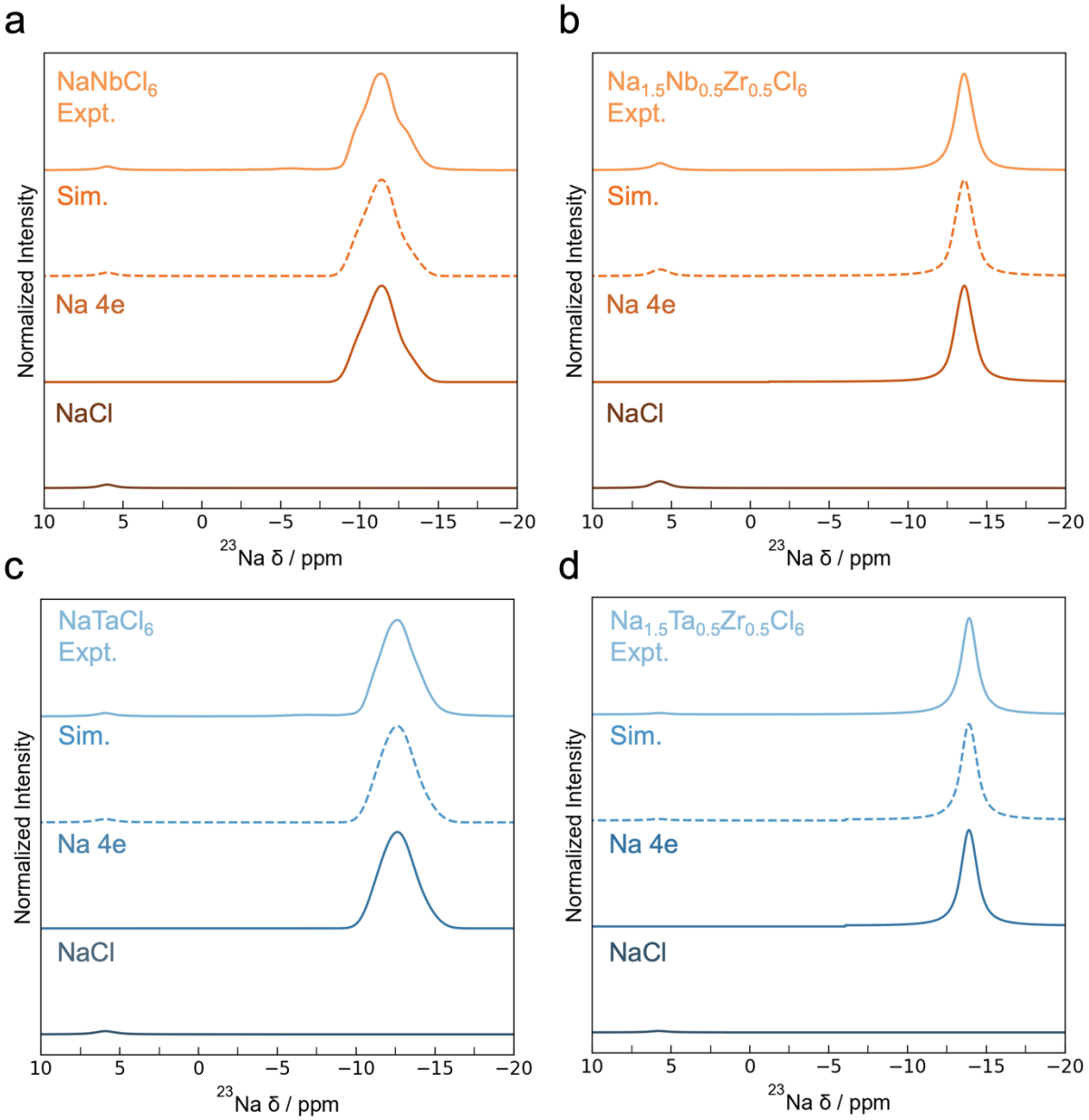

Supplementary Figure S6. ^{23}Na solid-state NMR spectra of a) $NaNbCl_6$, b) $Na_{1.5}Nb_{0.5}Zr_{0.5}Cl_6$, c) $NaTaCl_6$, and d) $Na_{1.5}Ta_{0.5}Zr_{0.5}Cl_6$. The simulated ^{23}Na spectra include sodium residing in the 4e site of the crystal structure and NaCl impurity.

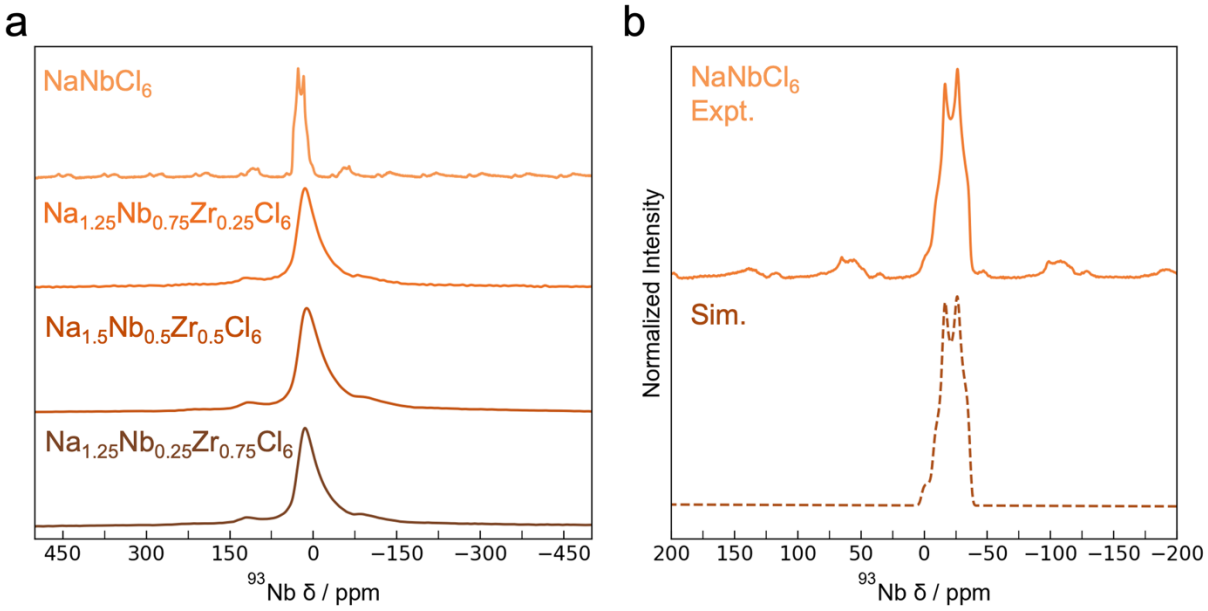

Supplementary Figure S7. a) ^{93}Nb solid-state NMR spectra collected on $Na_{2-x}Nb_xZr_{1-x}Cl_6$ solid-solutions. b) Simulated ^{93}Nb NMR centerband of niobium residing in the 4e site of the crystal structure.

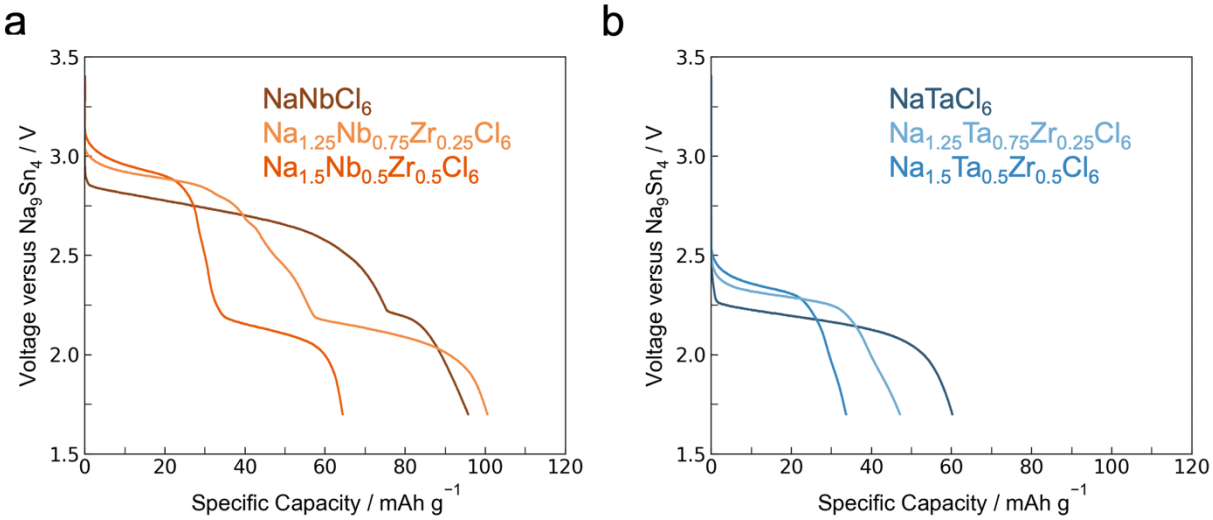

Supplementary Figure S8. First sodiation voltage profile for a) $Na_{2-x}Nb_xZr_{1-x}Cl_6$ (x = 1, 0.75, 0.5) and b) $Na_{2-x}Ta_xZr_{1-x}Cl_6$ (x = 1, 0.75, 0.5, 0.25) catholytes.

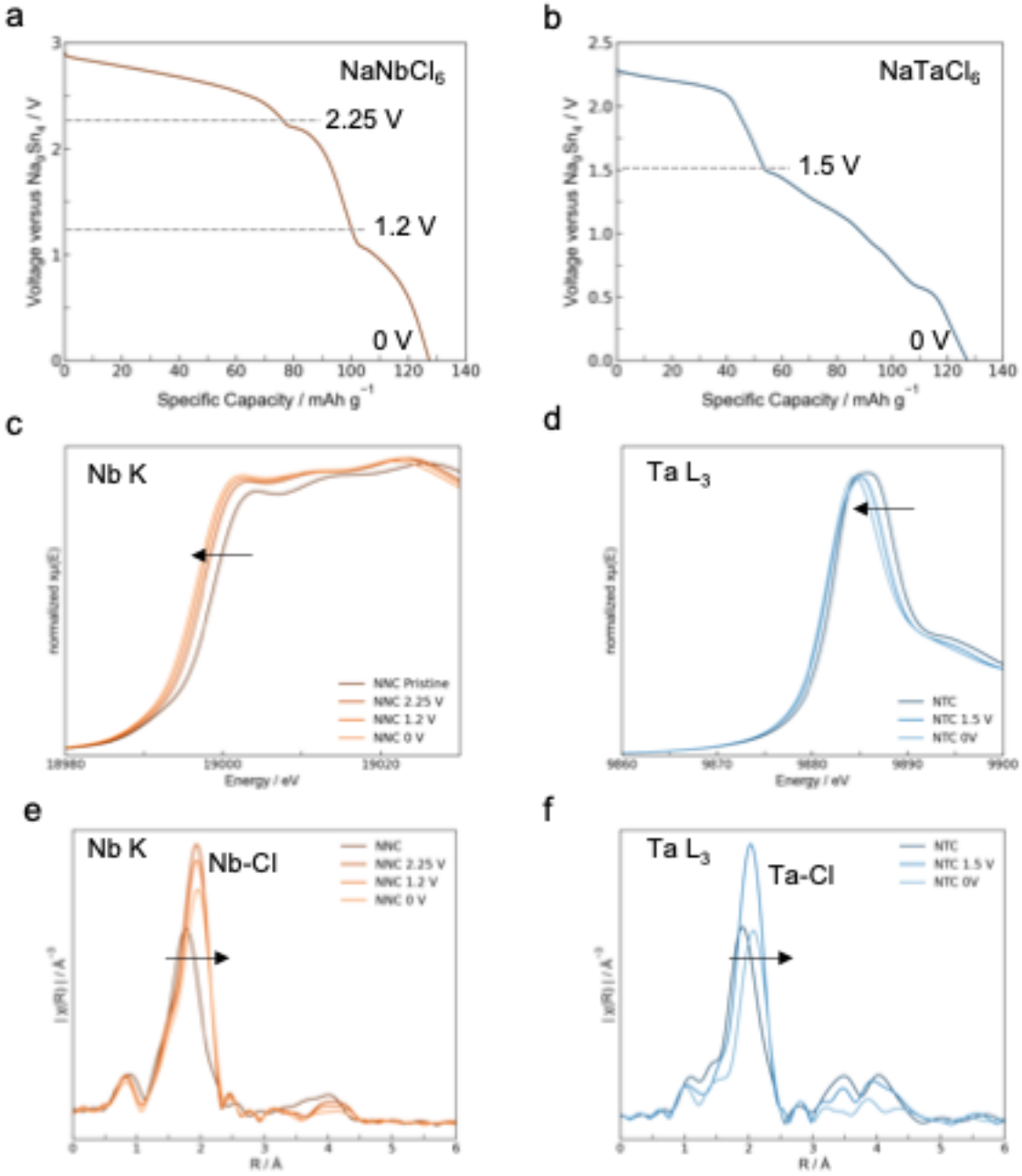

Supplementary Figure S9. Discharge voltage profiles for a) $NaNbCl_6$ and b) $NaTaCl_6$ electrodes. c) Normalized Nb K-edge XANES spectra, d) normalized Ta L3-edge spectra, K3-weighted Fourier transform magnitudes of e) Nb K-edge, f) Ta L3-edge spectra of pristine and reduced $NaNbCl_6$ and $NaTaCl_6$ powders.

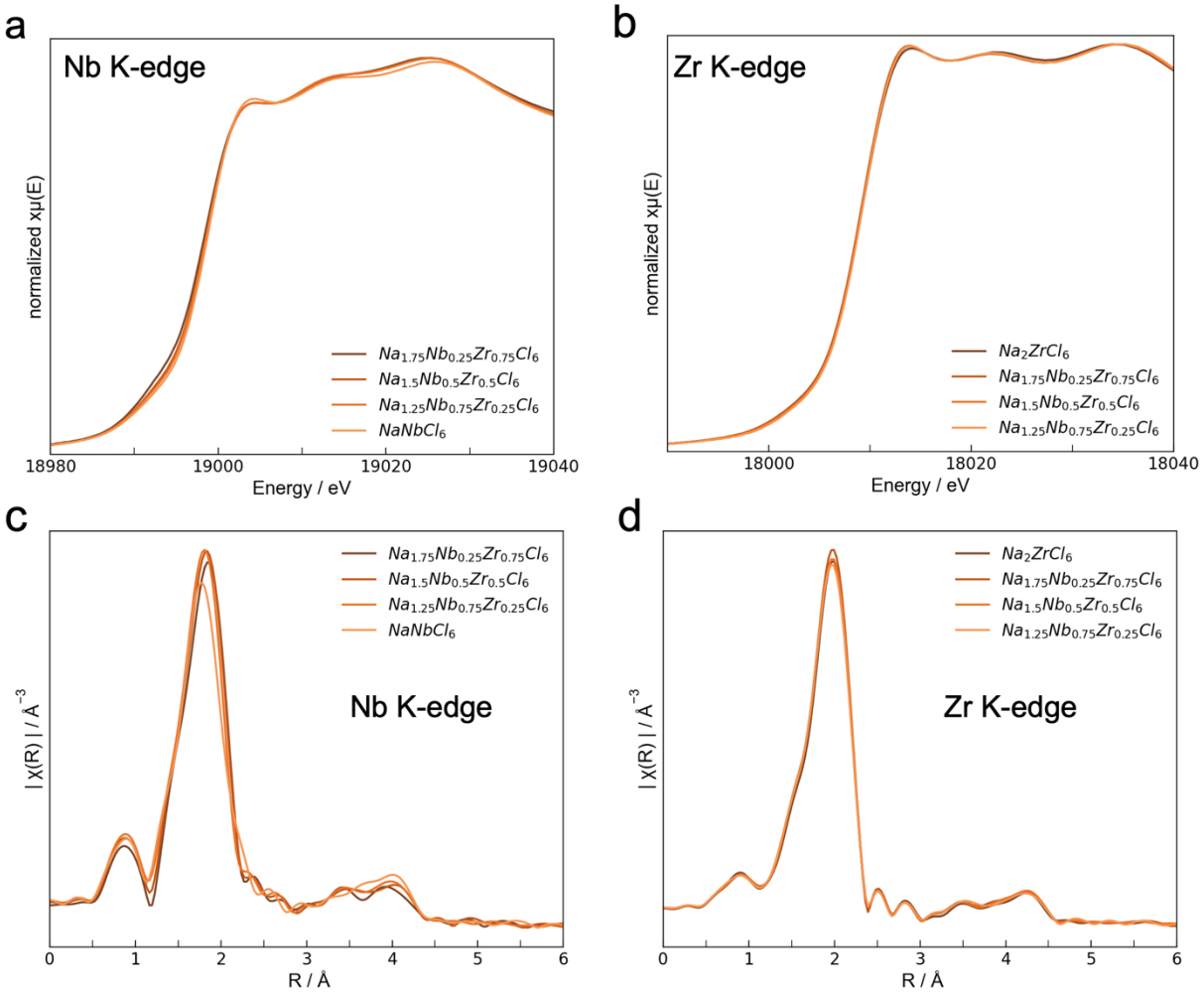

Supplementary Figure S10. Normalized a) Nb K-edge and b) Zr K-edge XANES spectra, K^3-weighted Fourier transform magnitudes of c) Nb K-edge and d) Zr K-edge spectra collected for $Na_{2-x}Nb_xZr_{1-x}Cl_6$ solid-solutions.

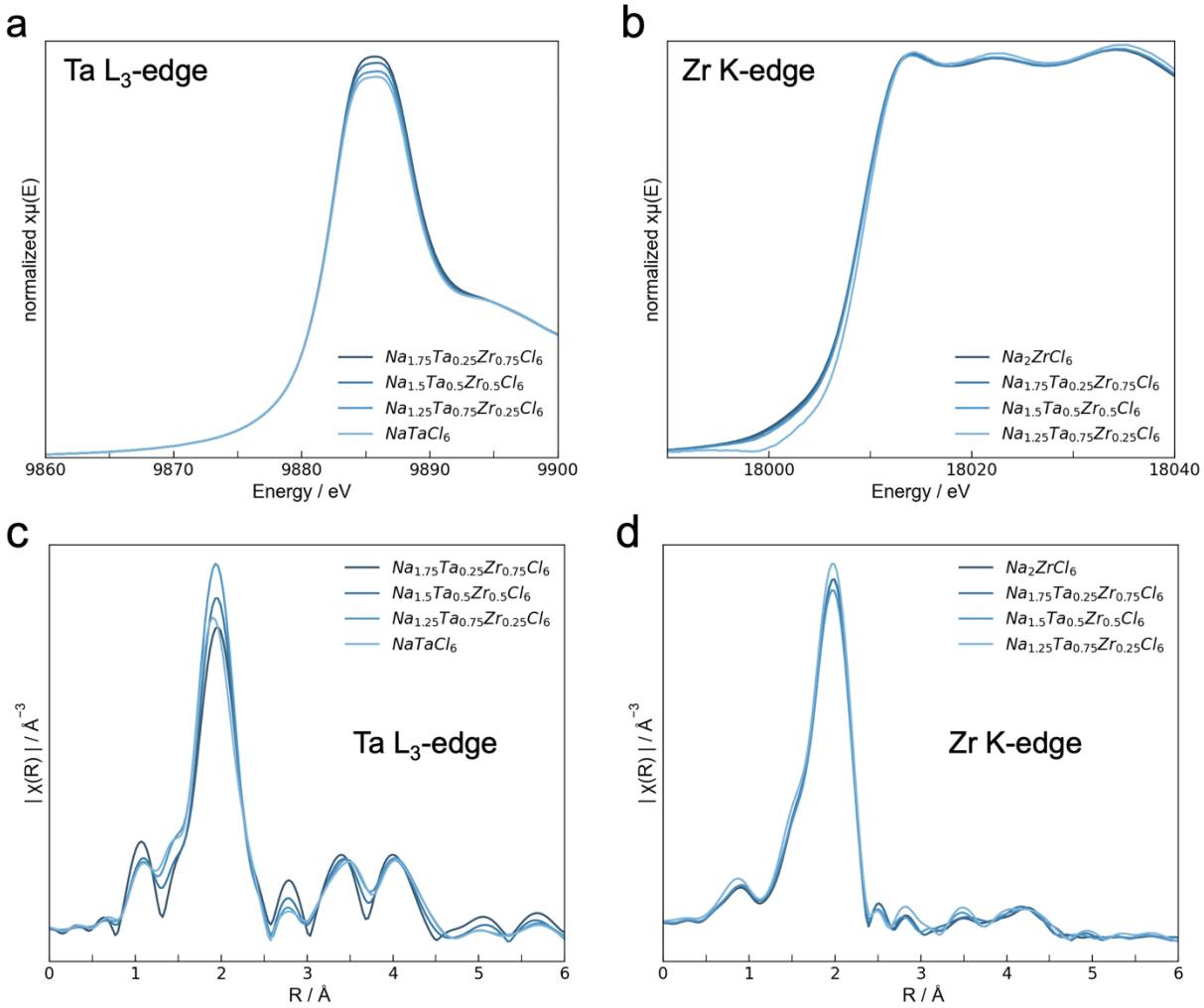

Supplementary Figure S11. Normalized a) Ta L_3-edge and b) Zr K-edge XANES spectra, K^3-weighted Fourier transform magnitudes of c) Ta L_3-edge and d) Zr K-edge spectra collected for $Na_{2-x}Ta_xZr_{1-x}Cl_6$ solid-solutions.

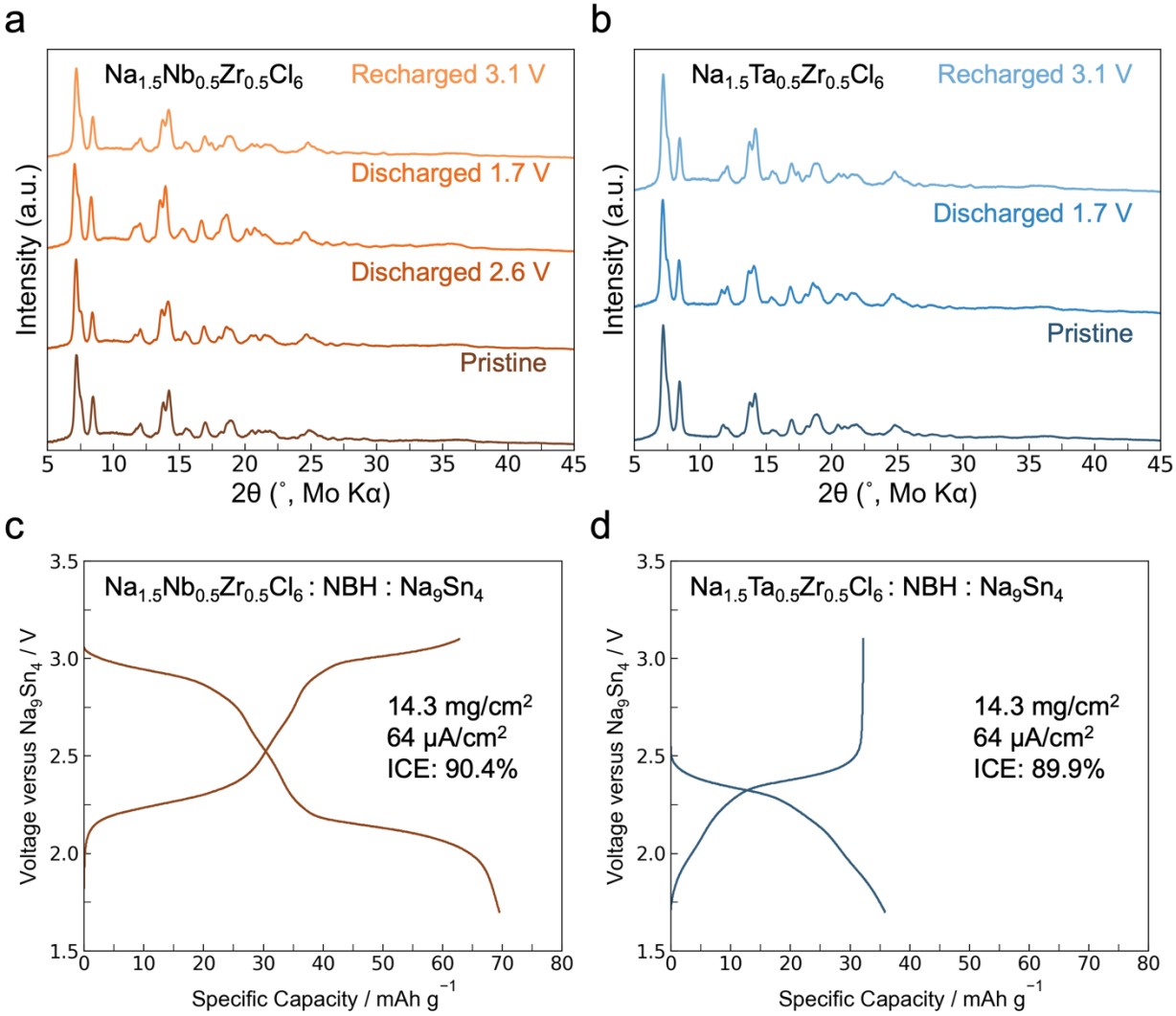

Supplementary Figure S12. X-ray diffraction patterns for pristine and sodiated a) $Na_{2-x}Nb_xZr_{1-x}Cl_6$ (x = 0.5) and b) $Na_{2-x}Ta_xZr_{1-x}Cl_6$ (x = 0.5) catholytes. First cycle voltage for half-cells consisting of c) $Na_{2-x}Nb_xZr_{1-x}Cl_6$ (x = 0.5) and d) $Na_{2-x}Ta_xZr_{1-x}Cl_6$ (x = 0.5) catholytes, cycled between 1.7–3.1 V vs. Na_9Sn_4.

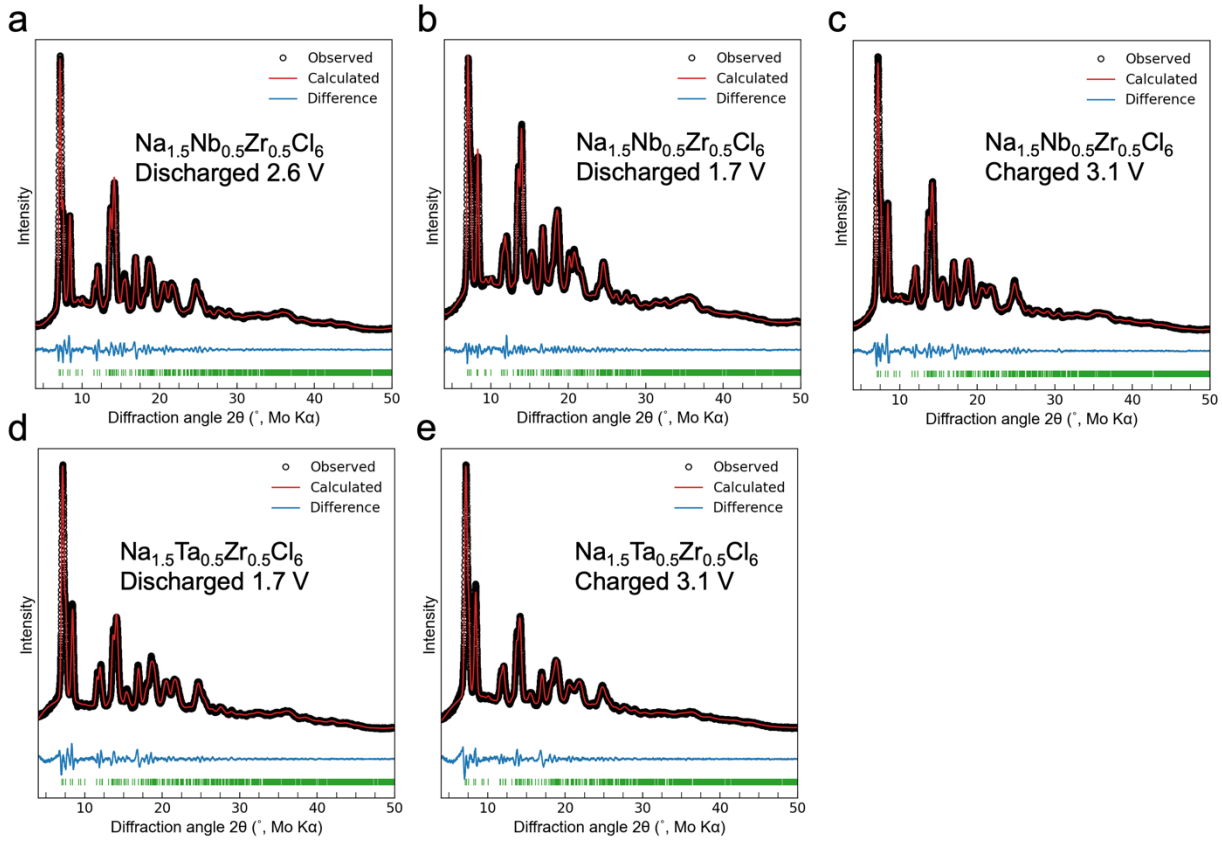

Supplementary Figure S13. Le Bail intensity fitting results for sodiated and desodiated a-c) $Na_{2-x}Nb_xZr_{1-x}Cl_6$ (x = 0.5) and d,e) $Na_{2-x}Ta_xZr_{1-x}Cl_6$ (x = 0.5) catholytes.

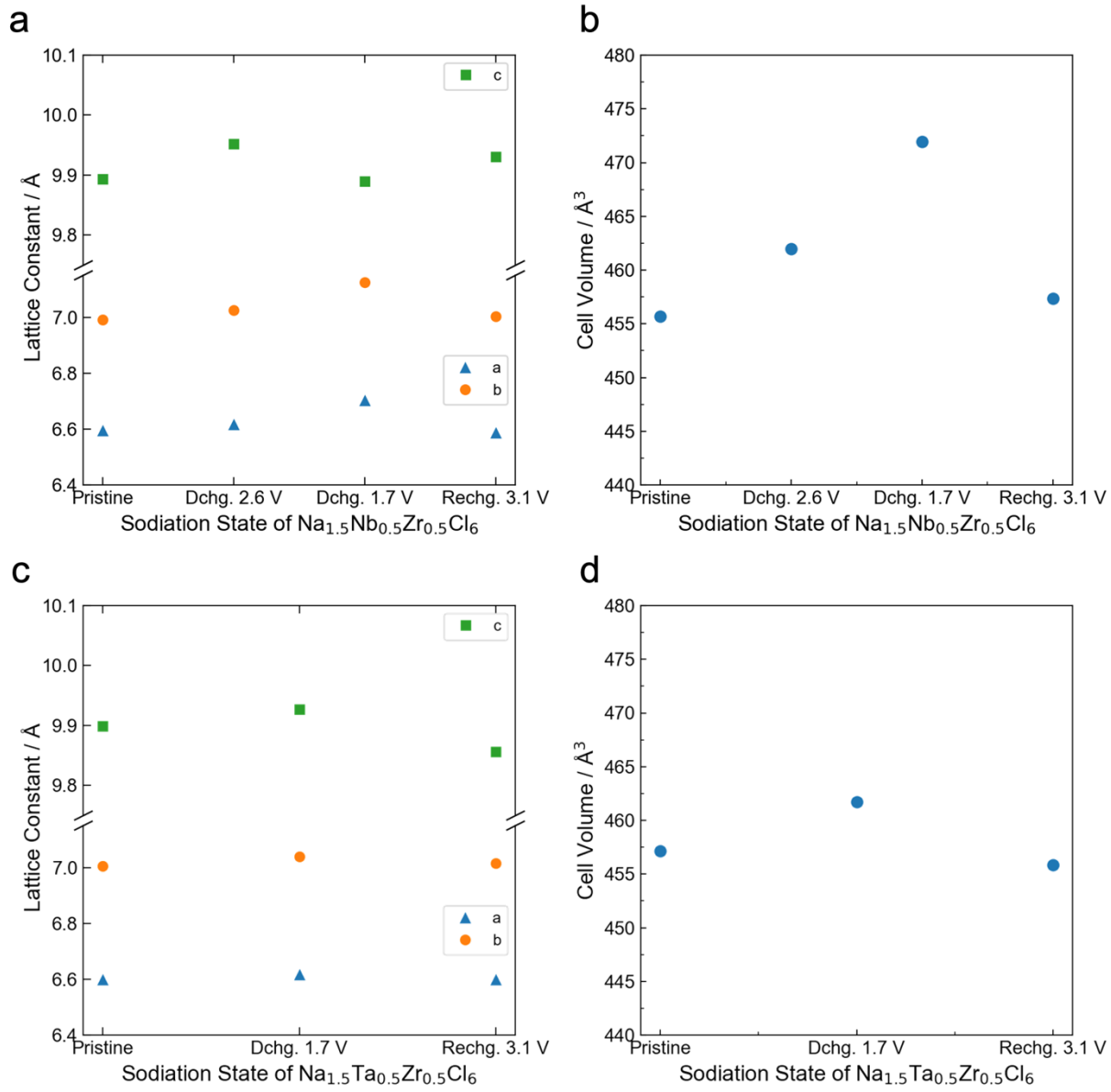

Supplementary Figure S14. Lattice constants extracted from Le Bail fits for a,b) $Na_{2-x}Nb_xZr_{1-x}Cl_6$ (x = 0.5) and c,d) $Na_{2-x}Ta_xZr_{1-x}Cl_6$ (x = 0.5) pristine, sodiated, and desodiated powders. Estimated standard deviations were too small to be graphically represented and are omitted.

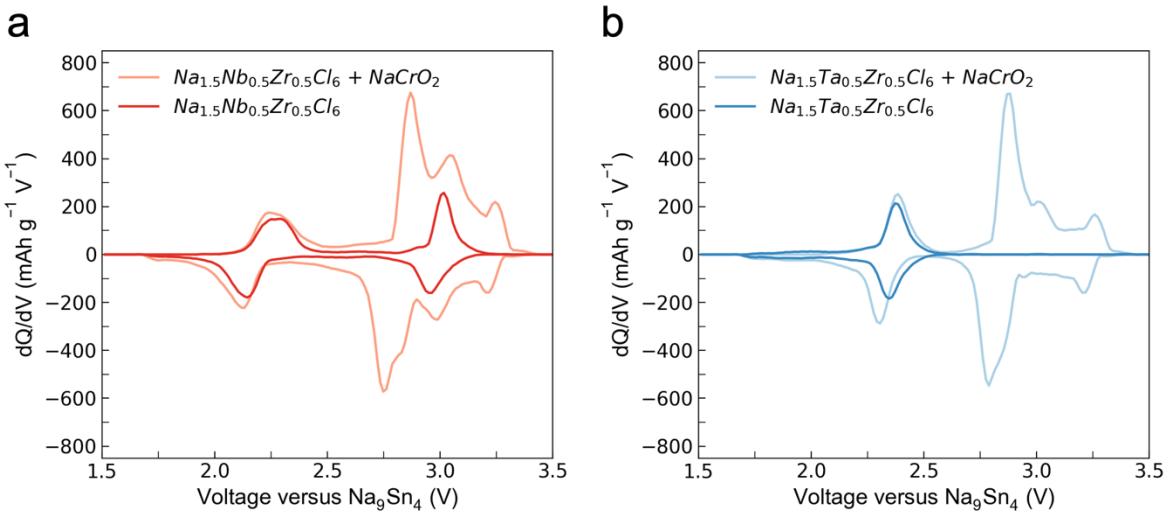

Supplementary Figure S15. Second cycle differential capacity plots of half-cell cathode composites consisting of a) $NaCrO_2$ mixed with $Na_{1.5}Nb_{0.5}Zr_{0.5}Cl_6$ and bare $Na_{1.5}Nb_{0.5}Zr_{0.5}Cl_6$ and b) $NaCrO_2$ mixed with $Na_{1.5}Ta_{0.5}Zr_{0.5}Cl_6$ and bare $Na_{1.5}Ta_{0.5}Zr_{0.5}Cl_6$.

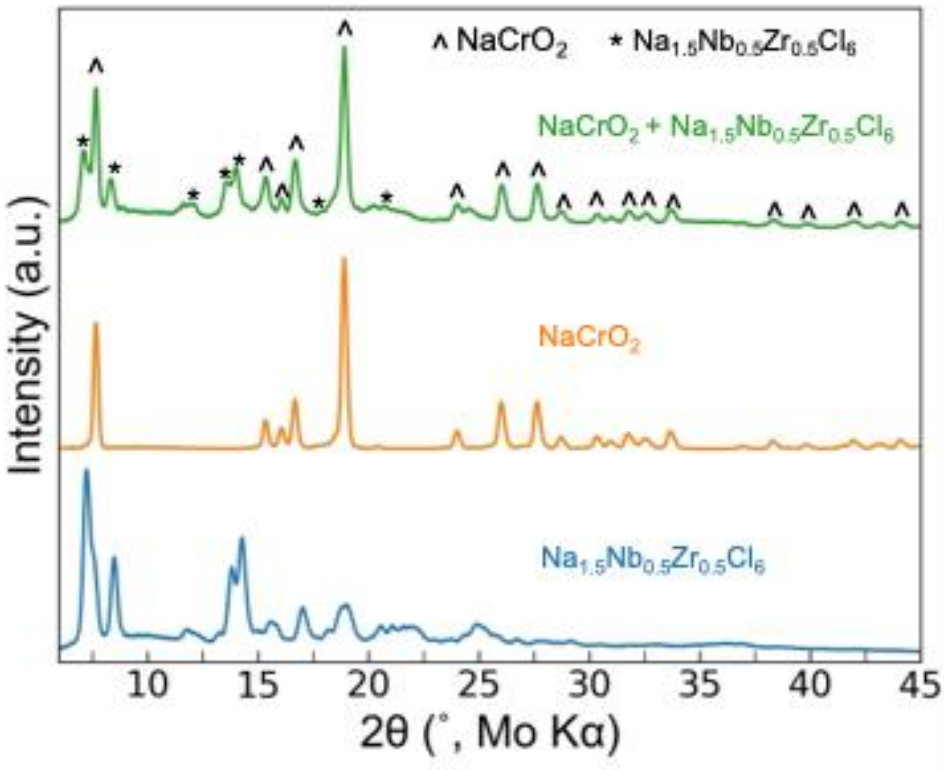

Supplementary Figure S16. X-ray diffraction patterns of pristine $Na_{1.5}Nb_{0.5}Zr_{0.5}Cl_6$ solid electrolyte, pristine $NaCrO_2$ cathode, and composite consisting of $Na_{1.5}Nb_{0.5}Zr_{0.5}Cl_6$ and $NaCrO_2$.

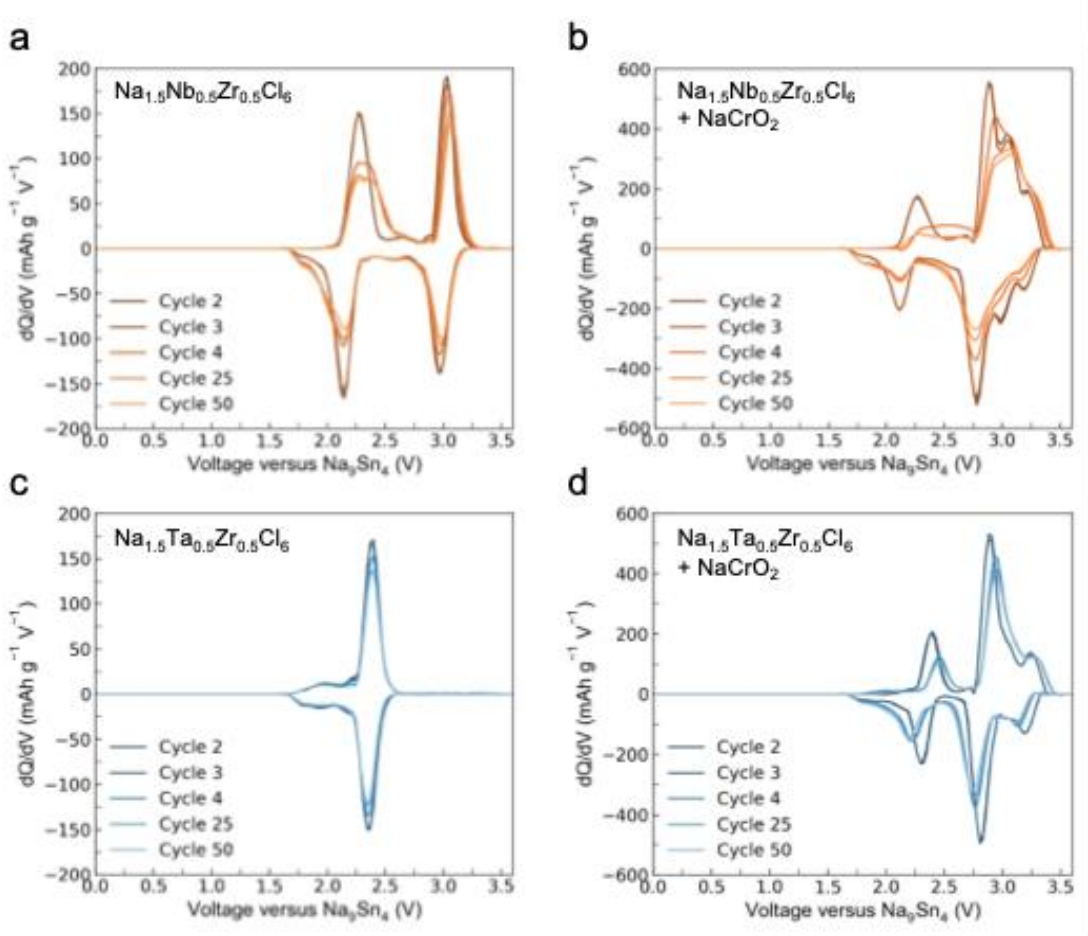

Supplementary Figure S17. X-ray diffraction patterns of pristine $Na_{1.5}Nb_{0.5}Zr_{0.5}Cl_6$ solid electrolyte, pristine $NaCrO_2$ cathode, and composite consisting of $Na_{1.5}Nb_{0.5}Zr_{0.5}Cl_6$ and $NaCrO_2$.

TABLES

Supplementary Table S1. Rietveld refinement results for $NaNbCl_6$ solid electrolyte fit against X-ray diffraction data collected using glass capillaries in Debye–Scherrer geometry.

Atom	Wyckoff position	Atomic coordinates			Occ.	U_{iso}
		x	*y*	*z*		
Na	4e	0.7801	0.3307	0.2454	1	0.0063
Nb	4e	0.2540	0.2236	0.1125	1	0.0406
Cl	4e	0.3740	0.1783	0.2287	1	0.0255
Cl	4e	0.5511	0.3982	0.0899	1	0.0120
Cl	4e	0.0956	0.4835	0.1529	1	0.0199
Cl	4e	0.1121	0.2557	0.0084	1	0.0169
Cl	4e	0.9595	0.0337	0.1535	1	0.0191
Cl	4e	0.4074	0.9284	0.0923	1	0.0155

Supplementary Table S2. Rietveld refinement results for $NaTaCl_6$ solid electrolyte fit against X-ray diffraction data collected using glass capillaries in Debye–Scherrer geometry.

Atom	Wyckoff position	Atomic coordinates			Occ.	U_{iso}
		x	*y*	*z*		
Na	4e	0.7697	0.3286	0.2504	1	0.0100
Ta	4e	0.3618	0.1692	0.2319	1	0.0114
Cl	4e	0.3618	0.1692	0.2319	1	0.0354
Cl	4e	0.5403	0.3858	0.0959	1	0.0092
Cl	4e	0.1036	0.4619	0.1548	1	0.0533
Cl	4e	0.0979	0.2619	0.0071	1	0.0583
Cl	4e	0.9669	0.0216	0.1577	1	0.0100
Cl	4e	0.4001	0.9098	0.0875	1	0.0283

Supplementary Table S3. Solid-state NMR spectra quantification results for each $Na_{2-x}Nb_xZr_{1-x}Cl_6$ composition with molar and weight percentages of the respective sample and NaCl impurity.

	Mol.% Sample	**Mol.% NaCl**	**Wt.% Sample**	**Wt.% NaCl**
$NaNbCl_6$	98.13	1.87	99.66	0.34
$Na_{1.25}Nb_{0.75}Zr_{0.25}Cl_6$	93.61	6.39	98.82	1.18
$Na_{1.5}Nb_{0.5}Zr_{0.5}Cl_6$	97.38	2.62	99.54	0.46
$Na_{1.75}Nb_{0.25}Zr_{0.75}Cl_6$	97.74	2.26	99.61	0.39
Na_2ZrCl_6	92.90	7.10	98.74	1.26

Supplementary Table S4. Solid-state NMR spectra quantification results for each $Na_{2-x}Ta_xZr_{1-x}Cl_6$ composition with molar and weight percentages of the respective sample and NaCl impurity.

	Mol.% Sample	**Mol.% NaCl**	**Wt.% Sample**	**Wt.% NaCl**
$NaTaCl_6$	98.19	1.81	99.74	0.26
$Na_{1.25}Ta_{0.75}Zr_{0.25}Cl_6$	99.43	0.57	99.92	0.08
$Na_{1.5}Ta_{0.5}Zr_{0.5}Cl_6$	98.39	1.61	99.75	0.25
$Na_{1.75}Ta_{0.25}Zr_{0.75}Cl_6$	97.65	2.35	99.62	0.38
Na_2ZrCl_6	92.90	7.10	98.74	1.26

Supplementary Table S5. Calculated and fitted chemical shifts and quadrupolar couplings for ^{23}Na nuclei in $NaNbCl_6$, $Na_{1.5}Nb_{0.5}Zr_{0.5}Cl_6$, $NaTaCl_6$, and $Na_{1.5}Ta_{0.5}Zr_{0.5}Cl_6$.

		Calculated					Experimental		
	Site	σ_{iso} **(ppm)**	δ_{aniso} **(ppm)**	η_{CS}	C_Q **(MHz)**	η_Q	δ_{iso} **(ppm)**	C_Q **(MHz)**	η_Q
$NaNbCl_6$	Na 4e	549.26	–12.71	0.13	0.907	0.51	–8.27(2)	0.906(4)	0.68(2)
NaCl	Na 4a						7.39(7)		
$Na_{1.5}Nb_{0.5}Zr_{0.5}Cl_6$	Na 4e	545.43	10.91	0.37	1.30	0.52	–11.88(2)		
NaCl	Na 4a						7.35(8)		
$NaTaCl_6$	Na 4e	551.10	–11.03	0.25	1.03	0.14	–9.73(2)	0.878(3)	0.60(1)
NaCl	Na 4a						7.40(8)		
$Na_{1.5}Ta_{0.5}Zr_{0.5}Cl_6$	Na 4e						–12.50(2)		
NaCl	Na 4a						6.89(2)		

Supplementary Table S6. Calculated and fitted chemical shieldings/shifts and quadrupolar coupling for ^{93}Nb nucleus in $NaNbCl_6$.

		Calculated					Experimental		
	Site	σ_{iso} **(ppm)**	δ_{aniso} **(ppm)**	η_{CS}	C_Q **(MHz)**	η_Q	δ_{iso} **(ppm)**	C_Q **(MHz)**	η_Q
$NaNbCl_6$	Nb 4e	–792.8	–89.65	0.90	9.219	0.94	39.0(2)	10.36(3)	0.45(1)

Supplementary Table S7. T_1 relaxation times of ^{23}Na for $Na_{2-x}M_xZr_{1-x}Cl_6$ (M = Nb, Ta, $0 \leq x \leq 1$).

	^{23}**Na** T_1**(s)**
$NaNbCl_6$	16
$Na_{1.25}Nb_{0.75}Zr_{0.25}Cl_6$	0.064
$Na_{1.5}Nb_{0.5}Zr_{0.5}Cl_6$	0.039
$Na_{1.75}Nb_{0.25}Zr_{0.75}Cl_6$	-
$NaTaCl_6$	3.26
$Na_{1.25}Ta_{0.75}Zr_{0.25}Cl_6$	0.056
$Na_{1.5}Ta_{0.5}Zr_{0.5}Cl_6$	0.014
$Na_{1.75}Ta_{0.25}Zr_{0.75}Cl_6$	0.019
Na_2ZrCl_6 $P2_1/n$	0.213
Na_2ZrCl_6 $P\bar{3}m1$	0.542 – 0.724

Supplementary Table S8. Specific capacity for one-electron and two-electron redox processes for $Na_{2-x}Nb_xZr_{1-x}Cl_6$ solid-solutions.

	Molecular Weight	**Specific Capacity / e$^-$**	**Specific Capacity / 2e$^-$**
	g·mol^{-1}	**mAh·g^{-1}**	**mAh·g^{-1}**
$Na_{1.75}Nb_{0.25}Zr_{0.75}Cl_6$	344.6	19.4	38.8
$Na_{1.5}Nb_{0.5}Zr_{0.5}Cl_6$	339.3	39.5	79.0
$Na_{1.25}Nb_{0.75}Zr_{0.25}Cl_6$	333.9	60.2	120.4
$NaNbCl_6$	328.6	81.6	163.2
$Na_{1.75}Ta_{0.25}Zr_{0.75}Cl_6$	366.6	18.3	36.6
$Na_{1.5}Ta_{0.5}Zr_{0.5}Cl_6$	383.3	35.0	70.0
$Na_{1.25}Ta_{0.75}Zr_{0.25}Cl_6$	400.0	50.3	100.6
$NaTaCl_6$	416.7	64.3	128.6

Supplementary Table S9. EXAFS fitting results for k^3-weighted Fourier transformed magnitudes of Nb K-edges, Zr K-edges, and Ta L_3-edges of pristine and sodiated $Na_{2-x}Nb_xZr_{1-x}Cl_6$ powders.

State	X-Y pair	CN	R	$\sigma^2/10^{-2}$	R-factor
Pristine	Nb-Cl	3	2.30(3)	0.05(4)	0.020
	Nb-Cl	3	2.43(3)	0.12(5)	
	Zr-Cl	6	2.471(5)	0.49(6)	0.005
2.6 V	Nb-Cl	6	2.428(8)	0.46(1)	0.016
	Zr-Cl	6	2.475(4)	0.45(5)	0.003
1.7 V	Nb-Cl	3	2.56(2)	0.21(4)	0.008
	Nb-Cl	3	2.44(2)	0.13(3)	
	Zr-Cl	6	2.477(4)	0.50(6)	0.004

Supplementary Table S10. EXAFS fitting results for k^3-weighted Fourier transformed magnitudes of Nb K-edges, Zr K-edges, and Ta L_3-edges of pristine and sodiated $Na_{2-x}Ta_xZr_{1-x}Cl_6$ powders.

State	X-Y pair	CN	R	$\sigma^2/10^{-2}$	R-factor
Pristine	Ta-Cl	3	2.32(2)	0.07(3)	0.013
	Ta-Cl	3	2.44(2)	0.16(4)	
	Zr-Cl	6	2.474(4)	0.51(5)	0.004
1.7 V	Ta-Cl	6	2.422(8)	0.38(1)	0.013
	Zr-Cl	6	2.479(3)	0.45(5)	0.003